

Internal nanoparticle structure of temperature-responsive self-assembled PNIPAM-b-PEG-b-PNIPAM triblock copolymers in aqueous solutions: NMR, SANS and light scattering studies

Article

Accepted Version

Filippov, S. K., Bogomolova, A., Kabarov, L., Velychkivska, N., Starovoytova, L., Cernochova, Z., Rogers, S. E., Lau, W. M., Khutoryanskiy, V. V. ORCID: <https://orcid.org/0000-0002-7221-2630> and Cook, M. T. (2016) Internal nanoparticle structure of temperature-responsive self-assembled PNIPAM-b-PEG-b-PNIPAM triblock copolymers in aqueous solutions: NMR, SANS and light scattering studies. *Langmuir*, 32 (21). pp. 5314-5323. ISSN 1520-5827 doi: 10.1021/acs.langmuir.6b00284 Available at <https://centaur.reading.ac.uk/65646/>

It is advisable to refer to the publisher's version if you intend to cite from the work. See [Guidance on citing](#).

To link to this article DOI: <http://dx.doi.org/10.1021/acs.langmuir.6b00284>

Publisher: American Chemical Society

All outputs in CentAUR are protected by Intellectual Property Rights law, including copyright law. Copyright and IPR is retained by the creators or other copyright holders. Terms and conditions for use of this material are defined in the [End User Agreement](#).

www.reading.ac.uk/centaur

CentAUR

Central Archive at the University of Reading

Reading's research outputs online

Internal nanoparticle structure of temperature-responsive self-assembled PNIPAM-*b*-PEG-*b*-PNIPAM triblock copolymers in aqueous solutions: NMR, SANS and Light Scattering studies

Sergey K. Filippov, Anna Yurevna Bogomolova, Leonid Kabarov, Nadiia Velychkivska, Larisa Starovoytova, Zulfiya Cernochova, Sarah E. Rogers, Wing Man Lau, Vitaliy V. Khutoryanskiy, and Michael T. Cook

Langmuir, **Just Accepted Manuscript** • DOI: 10.1021/acs.langmuir.6b00284 • Publication Date (Web): 09 May 2016

Downloaded from <http://pubs.acs.org> on May 16, 2016

Just Accepted

"Just Accepted" manuscripts have been peer-reviewed and accepted for publication. They are posted online prior to technical editing, formatting for publication and author proofing. The American Chemical Society provides "Just Accepted" as a free service to the research community to expedite the dissemination of scientific material as soon as possible after acceptance. "Just Accepted" manuscripts appear in full in PDF format accompanied by an HTML abstract. "Just Accepted" manuscripts have been fully peer reviewed, but should not be considered the official version of record. They are accessible to all readers and citable by the Digital Object Identifier (DOI®). "Just Accepted" is an optional service offered to authors. Therefore, the "Just Accepted" Web site may not include all articles that will be published in the journal. After a manuscript is technically edited and formatted, it will be removed from the "Just Accepted" Web site and published as an ASAP article. Note that technical editing may introduce minor changes to the manuscript text and/or graphics which could affect content, and all legal disclaimers and ethical guidelines that apply to the journal pertain. ACS cannot be held responsible for errors or consequences arising from the use of information contained in these "Just Accepted" manuscripts.



1
2
3
4
5
6 Internal nanoparticle structure of temperature-
7
8
9
10 responsive self-assembled PNIPAM-*b*-PEG-*b*-
11
12
13
14 PNIPAM triblock copolymers in aqueous
15
16
17
18 solutions: NMR, SANS and Light Scattering
19
20
21
22 studies
23
24
25
26

27 *Sergey K. Filippov*^{*,†}, *Anna Bogomolova*[†], *Leonid Kaberov*[†], *Nadiia Velychkivska*[†], *Larisa*
28 *Starovoytova*[†], *Zulfiya Cernochova*[†], *Sarah E. Rogers*[‡], *Wing Man Lau*^{||}, *Vitaliy V.*
29 *Khutoryanskiy*^{||}, *Michael T. Cook*^{*,⊥}
30
31
32
33
34

35 [†]Institute of Macromolecular Chemistry, AS CR, Heyrovsky Sq. 2, Prague, Prague 6, 162 06,
36
37 Czech Republic.
38
39

40 [‡]ISIS-STFC, Rutherford Appleton Laboratory, Chilton, OX11 0QX, Oxon, United Kingdom
41
42

43 ^{||} School of Pharmacy, University of Reading, Whiteknights, PO Box 224, Reading,
44
45 Berkshire, United Kingdom, RG6 6AD
46
47
48

49 [⊥] Department of Pharmacy & Research Centre in Topical Drug Delivery and Toxicology,
50
51 University of Hertfordshire, Hatfield, Hertfordshire, United Kingdom, AL10 9AB
52
53
54
55
56
57
58
59
60

KEYWORDS: nanoparticles, copolymers; NMP; SANS; self-assembly; PNIPAM; microgel; light scattering

ABSTRACT

In this study we report detailed information on the internal structure of PNIPAM-*b*-PEG-*b*-PNIPAM nanoparticles formed from self-assembly in aqueous solutions upon increase in temperature. NMR spectroscopy, light scattering and small-angle neutron scattering (SANS) were used to monitor different stages of nanoparticle formation as a function of temperature, providing insight into the fundamental processes involved. The presence of PEG in a copolymer structure significantly affects the formation of nanoparticles, making their transition to occur over a broader temperature range. The crucial parameter that controls the transition is the ratio of PEG/PNIPAM. For pure PNIPAM, the transition is sharp; the higher the PEG/PNIPAM ratio results in a broader transition. This behavior is explained by different mechanisms of PNIPAM block incorporation during nanoparticle formation at different PEG/PNIPAM ratios. Contrast variation experiments using SANS show that the structure of nanoparticles above cloud point temperatures for PNIPAM-*b*-PEG-*b*-PNIPAM copolymers is drastically different from the structure of PNIPAM mesoglobules. In contrast with pure PNIPAM mesoglobules, where solid-like particles and chain network with a mesh size of 1-3 nm are present; nanoparticles formed from PNIPAM-*b*-PEG-*b*-PNIPAM copolymers have non-uniform structure with “frozen” areas interconnected by single chains in Gaussian conformation. SANS data with deuterated “invisible” PEG blocks imply that PEG is uniformly distributed inside of a nanoparticle. It is kinetically flexible PEG blocks which affect the nanoparticle formation by prevention of PNIPAM microphase separation.

INTRODUCTION

Temperature-responsive polymers are a class of materials which undergo phase changes upon heating or cooling their solutions. If a polymer displays an expanded coil to globule transition during heating, associated with reduced solubility, it is said to display cloud point temperature (CPT). A phase diagram for aqueous solutions of temperature-responsive polymers is characterized by so-called lower critical solution temperature (LCST).^{1,2} This transition occurs due to an unfavourable entropy of mixing. A polymer reaching its CPT is usually associated with an increase in solution turbidity due to the collapse of the expanded coil, resulting in a globule which is able to phase separate via a mesoglobular state, which subsequently scatters light. For a homopolymer, the final result of reaching the CPT is polymer phase separation in solution. In block copolymer solutions, however, the phase separation of one block can result in the formation of a self-assembled structure – including micelles,³⁻¹⁰ worm-like micelles,¹¹ and gels.¹² These self-assembled structures have potential use in drug delivery, releasing their load in a temperature-dependent fashion.¹³

Poly(N-isopropyl acrylamide) (PNIPAM) is one of the most highly studied temperature-responsive polymers exhibiting a LCST. The LCST of a PNIPAM homopolymer is approximately 32°C, though copolymerization with hydrophilic monomers may alter this, as well as changes in concentration, ionic strength, and pH.¹⁴ Diblock copolymers of poly(ethylene glycol) (PEG) and PNIPAM are able to form micelles,¹⁵⁻¹⁸ vesicles,^{19,20} and gels,^{21,22} depending on molecular weights and concentration. It was established that vesicles are formed from a three-level intermediate hierarchical structure that exist in solution below CPT.²⁰ ABA triblock copolymers of PNIPAM-*b*-PEG-*b*-PNIPAM have been less studied,^{22,23} and are known to form both micelles¹⁵ and gels.^{21,22} At high concentrations of block copolymer (> 20 wt.%), gels are formed, depending on the molecular weight of each block.²¹ At lower concentrations shorter block length is detrimental to gel formation. Topp et al¹⁵ used cerium to initiate chain growth of PNIPAM (1.6 kDa) from PEG (6 kDa) to give ABA

triblock copolymers which assembled into micelles above 30.9°C. This was not an extensive study, but to our knowledge is the first report of these materials. However, the effect of molecular weight of each block was not determined. Previously, Hennik *et.al.*²³ studied PNIPAM-*b*-PEG-*b*-PNIPAM copolymers and the presence of flower-like micelles in solution was reported above CPT in contrast with ordinary micelles formed by PEG-*b*-PNIPAM copolymers. Existence of loops in flower-like micelles was convincingly demonstrated by ¹H NMR relaxometry.²³

In this study we use small-angle neutron scattering (SANS), light scattering and NMR to study the formation of nanoparticles from PNIPAM-*b*-PEG-*b*-PNIPAM block copolymers. The main difference of PNIPAM-*b*-PEG-*b*-PNIPAM block copolymers reported here from ones reported in references^{19,20,23} is much shorter length of PNIPAM block. This allows for comprehensive study of the internal structure of these self-assembled nanostructures, as well as the other features occurring during self-assembly.

Materials

Tris(2-aminoethyl)amine (TREN), polyethylene glycol (PEG, 4 kDa), α -bromoisobutyryl bromide (BIBB), formic acid, formaldehyde, N-isopropyl acrylamide (NIPAM), and copper (I) chloride were purchased from Sigma-Aldrich (U.K.). Deuterated PEG (3.5 kDa) was purchased from Polymer Source (Canada). Dialysis membranes with a 3.5 kDa molecular weight cut-off (MWCO) were purchased from Visking (U.K.) and soaked for 1 h in deionized water prior to use. Toluene and triethylamine were dried over 3 Å molecular sieves for 24 h prior to use.

Methods

Synthesis of PNIPAM-*b*-PEG-*b*-PNIPAM triblock copolymers via atom-transfer radical-polymerization (ATRP)

ATRP was conducted using the difunctionalized PEG macroinitiator and Me₆TREN catalyst described above, with an initiator:catalyst:ligand ratio of 1:1:1. The ATRP procedure was as follows: CuCl (12.4 mg, 125 μmol) was placed into a round-bottom flask, sealed with a septum, then purged with N₂ for 20 min. A second flask was prepared containing NIPAM (500 mg for 'low' Mw PNIPAM or 1.25 g for 'high' Mw PNIPAM) and PEG macroinitiator (500 mg, 125 μmol). H₂O (2 mL) was added, followed by Me₆TREN (33.4 μL, 28.8 mg, 125 μmol). The solution was then allowed to stir at room temperature until complete dissolution (c.a. 5 min). The solution containing NIPAM, macroinitiator, and ligand was then bubbled through with N₂ for 20 min, at which point it was transferred to the flask containing CuCl via syringe. The reaction was then allowed to proceed at room temperature for 24 h with stirring. The resulting blue-green solution was concentrated *in vacuo*, dissolved in tetrahydrofuran (THF) (5 mL), then passed through a short length of neutral alumina, resulted in a colourless solution. This was concentrated *in vacuo* to yield a white solid, PNIPAM-b-PEG-b-PNIPAM. Dialysis (MWCO 3.5 kDa) was necessary to remove residual monomers (as detected by ¹H NMR). ¹H NMR (400 MHz, D₂O, δ): 3.86 (br, CH PNIPAM), 3.66 (br, CH₂ PEG), 1.97 (br, CH₂ PNIPAM), 1.54 (br, CH₂ PNIPAM), 1.11 (br, CH₃ PNIPAM) ppm.

Gel-permeation chromatography (GPC)

GPC was conducted in order to determine polydispersity indexes (PDIs) and confirm that PEG and PNIPAM blocks were bonded to each other. An Agilent 1260 Infinity GPC-SEC system combined with 1 x Waters Styragel HR2 column was used. THF was used as mobile phase at a flow rate of 1.0 mL min⁻¹. Polystyrene standards and samples were dissolved in THF (2 mg/mL) with gentle heating to ensure complete dissolution of PEG. *M_n* values quoted are determined by relative, narrow standard, calibration.

Nuclear Magnetic Resonance (NMR)

To characterize the behavior of the polymer system, the ^1H and ^1H spin-spin relaxation times T_2 were measured using NMR spectroscopy. Relaxation NMR spectroscopy is a useful tool for investigating polymer and solvent dynamics due to the fact that the transverse magnetization component is sensitive to changes in the mobility of polymer segments as well as the solvent.^{10, 24-26}

^1H NMR measurements were performed with a Bruker Avance III 600 spectrometer operating at 600.2 MHz. The integrated intensities were determined with the spectrometer integration software at an accuracy of $\pm 1\%$. In all measurements, the temperature was maintained at a constant value within ± 0.2 °C using a BVT 3000 temperature unit. The samples were kept at the experimental temperature for at least 15 min before the measurement. The measurement conditions were as follows: 90 pulses with a width of 10 μs , relaxation delay of 10 s, spectral width of 4844.961 Hz and 8 scans in the temperature range 17-57 °C. The ^1H spin-spin relaxation times T_2 for all components were measured using the CPMG pulse sequence $90^\circ \text{ x}-(t_d-180^\circ \text{ y}-t_d)_n$ -acquisition with $t_d = 0.5$ ms. Each experiment was conducted with 4 scans, a relaxation delay of 80 s and a spectral width of 9014.423 Hz. The obtained T_2 relaxation curves were monoexponential and the fitting process made it possible to determine a single value of the relaxation time. The relative error for T_2 values of PNIPAM, HDO and PEG protons did not exceed $\pm 8\%$, $\pm 5\%$ and $\pm 6\%$, respectively.

To quantitatively characterize the phase separation, we have used the values of the phase-separated fraction p obtained as

$$p(T) = 1 - \frac{I}{I_0} \quad (1)$$

where I is the integrated intensity of the given polymer signal in the spectrum of the partly separated system and I_0 is the integrated intensity of this signal if no phase separation occurs. For I_0 , we took values based on integrated intensities below the phase transition, using the

expected $1/T$ temperature dependence. The integrated intensities were measured ~ 20 min after the corresponding temperature was reached (by heating).

Small-angle neutron scattering (SANS)

SANS experiments were performed on the time-of-flight Sans2d diffractometer at the ISIS neutron facility, U.K. A simultaneous Q -range of $0.005 - 0.85 \text{ \AA}^{-1}$ was achieved by utilizing an incident wavelength range of $1.75 - 16.5 \text{ \AA}$ and employing an instrument set-up of $L_1 = L_2 = 4\text{ m}$ with the detector offset vertically 75 mm and sideways 305 mm . The beam diameter was 8 mm . Each scattering data set was corrected for the detector efficiencies, sample transmission and background scattering and converted to scattering cross-section data using instrument specific software.²⁷ These data were placed on an absolute scale (cm^{-1}) using the scattering from a standard sample (a solid blend of hydrogenous and perdeuterated polystyrene) in accordance with established procedures.²⁸ All solutions for SANS experiments were prepared using D_2O as solvent to reduce incoherent scattering. The concentrations of all solutions was $0.5 \text{ wt.}\%$. Scattering from pure D_2O was measured separately and subtracted from solution scattering data.

Light Scattering

Static and Dynamic Light scattering (SLS and DLS) was performed to characterize the micelles in dilute solutions. Initially, the pH dependency of the hydrodynamic radius of particles, R_h , and the scattering intensity, I_s , were measured at a scattering angle of $\theta = 173^\circ$ with a Zetasizer Nano-ZS instrument, Model ZEN3600 (Malvern Instruments, UK). The DTS (Nano) program was used to evaluate the data. It provides intensity-, volume-, and number-weighted R_h distribution functions $G(R_h)$.²⁹ The intensity-weighted value of the apparent R_h was chosen to monitor the temperature-dependent changes in the system.

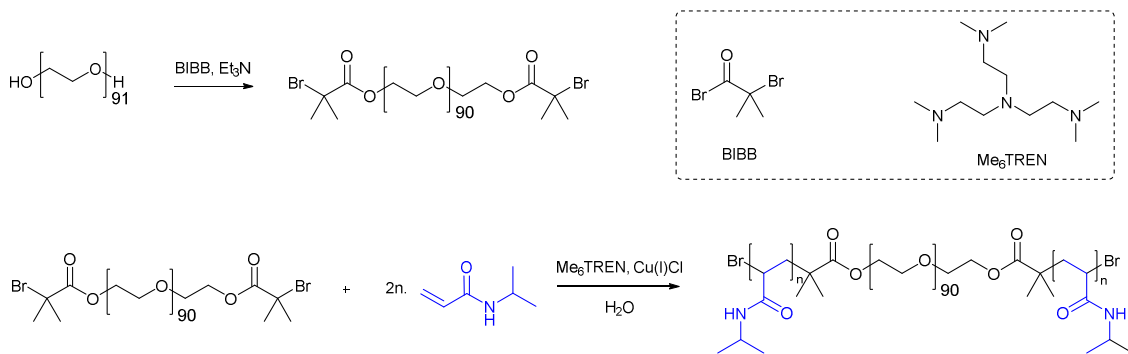
Static light scattering

The static light scattering measurements were performed at 40°C in the angular range 40-140° using ALV goniometer equipped with a 30 mW He-Ne laser ($\lambda = 632.8$ nm). Data evaluation was carried out through using Guinier and Berry models.³⁰ The differential index of refraction (dn/dc) was determined in a BI-DNDCW differential refractometer (Bruckhaven Instruments Corporation) at 620.0 nm, with Differential Refractometer Software. Stock solutions of PNIPAM-b-PEG-b-PNIPAM copolymers were prepared in D₂O (1 g/dm³). The dn/dc value was found to be around 1.45×10^{-4} L/g.

3D-DLS

The aforementioned system is relatively turbid, denoting the existence of multiple scattering contributions. Therefore the undesired multiple scattering contributions should be suppressed in order to get reliable measurements of the form factor, in diluted solutions, or of the structure factor in more concentrated ones.³¹⁻³³ Thus, the 3D-DLS cross-correlation technique was used where the scattering intensity from two beams of the same wavelength corresponding to the same scattering vector, but different scattering planes on the same scattering volume are cross-correlated. It has been shown that contributions from multiple scattering events is eliminated in this way, enabling us to extract information on only the single scattering contribution. The experimental set-up which was used for both DLS and SLS measurements is the 3D LS Spectrometer from LS instruments consisting of a goniometer system equipped with a single laser beam (Lumentum 1145/P HeNe laser 21mW) at 632.8nm. Experiments were conducted at 40 °C.

RESULTS AND DISCUSSION



Scheme 1. Synthetic route to PNIPAM-*b*-PEG-*b*-PNIPAM triblock copolymers

PNIPAM-*b*-PEG-*b*-PNIPAM triblock copolymers were synthesized using ATRP polymerization from a difunctionalized PEG macroinitiator (Scheme 1). This synthesis was conducted in aqueous conditions, using Me₆TREN as a ligand for a copper (I) chloride catalyst, which has been reported for the polymerization of PNIPAM.³⁴ Oxidation of copper (I) to copper (II) during the polymerization leads to the appearance of a blue-green colour solution, which was removed by passage through a short length of neutral alumina. ¹H NMR (Figure 1) showed that polymerization had occurred, with vinylic protons of the acrylamide moiety not present, replaced with alkyl protons at 1.97 and 1.54 ppm, corresponding to the polymer backbone. Additional characteristic broad peaks were identified for PNIPAM at 3.86 (CH) and 1.11 (CH₃) ppm, as well as the CH₂ protons for PEG at 3.66 ppm.

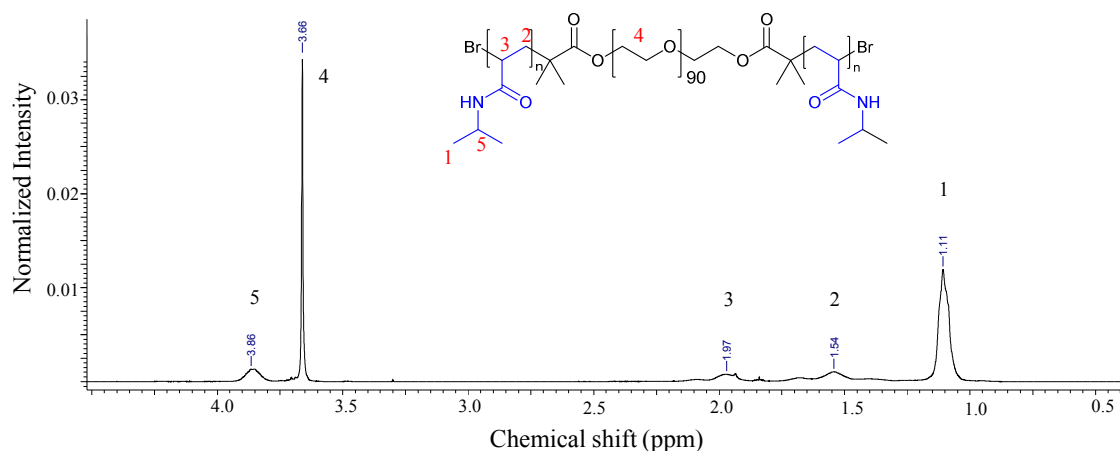


Figure 1. Exemplar ^1H NMR of PNIPAM-*b*-PEG-*b*-PNIPAM, displaying characteristic peaks of both PEG and PNIPAM.

Four samples were produced in total, in which the PEG blocks were either deuterated or non-deuterated, with PNIPAM blocks of two different molecular weights as determined by GPC (Table 1). These four samples can be grouped into two pairs. **A** and **B** have matched molecular weight deuterated-PEG and PEG blocks (3.5 and 4 kDa, respectively) and ‘short’ PNIPAM blocks (3.4 and 4.3 kDa, respectively). **C** and **D** have matched molecular weight deuterated-PEG and PEG blocks (3.5 and 4 kDa, respectively) and ‘long’ PNIPAM blocks (6.2 and 5.8 kDa, respectively). All products had satisfactory PDIs (< 1.4), considering the polydispersities of the macroinitiators.³⁴

Table 1. Molecular weight and PDI of PNIPAM-*b*-PEG-*b*-PNIPAM triblock copolymers

| Sample ID | Mn (kDa) | PDI | Mn of PEG (kDa, manufacturer) | Mn of PNIPAM blocks (kDa) GPC | N of PNIPAM blocks | N of PEG blocks |
|-----------|----------|-----|-------------------------------|-------------------------------|--------------------|-----------------|
| A | 10.3 | 1.4 | 3.5 [§] | 3.4 | 30 | 79 |
| B | 12.5 | 1.3 | 4.0 | 4.3 | 38 (43*) | 90 |
| C | 15.8 | 1.2 | 3.5 [§] | 6.2 | 54 | 79 |
| D | 15.5 | 1.2 | 4.0 | 5.8 | 51(60*) | 90 |

*- Data from NMR in D_2O ; [§]- PEG is deuterated

Dynamic light scattering experiments directly prove the presence of nanoparticles in solution at high temperature (Figure 2). A sharp transition is seen at the CPT of PNIPAM (approximately 35 °C), resulting in the formation of nanoparticles with a hydrodynamic radius (R_h) of approximately 75 nm. It should be noted here, that a low fraction of 200-300 nm aggregates were seen at low temperatures. This peak was discarded on Figure 2 due to concentration of these aggregates in solution is negligible. Above the CPT, the distribution was monomodal.

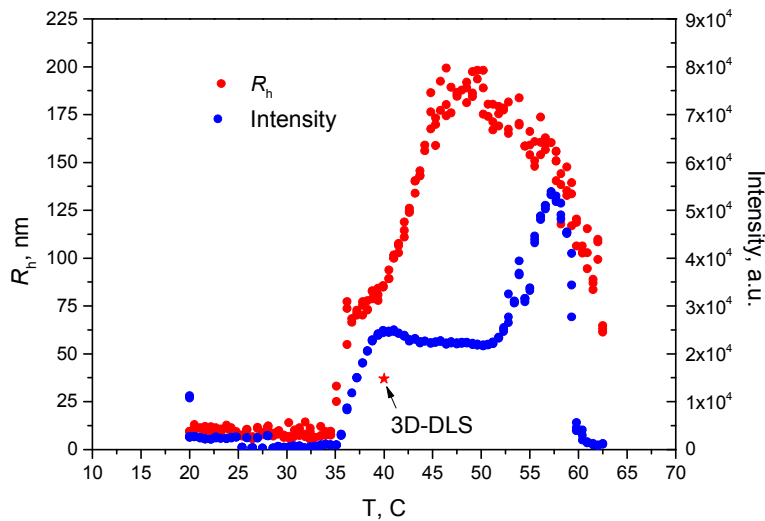


Figure 2. Temperature dependence of apparent hydrodynamic radius and scattered intensity for sample D measured using conventional DLS at $c=1.0$ wt.%. Star point indicated by arrow is the hydrodynamic radius value measured by 3D-DLS method.

Further heating above CPT, results in continuous increase in the apparent hydrodynamic radius up to 200 nm at approximately 50 °C followed by a significant drop to 50 nm. This behavior has been seen for different thermosensitive polymers such as glycogen-graft-poly(2-alkyl-2-oxazolines),³⁵ amphiphilic polyoxazolines,^{6,10} thermoresponsive nanoparticles based on poly(2-alkyl-2-oxazolines) and Pluronic F127,⁷ PNIPAM-g-PEO,³⁶ and poly(vinyl methyl

ether).³⁷ The growth of nanoparticles size can be explained by the increasing aggregation number of formed nanoparticles. At elevated temperatures, above 50°C, nanoparticle shrinks with increasing of temperature due to worsening of the thermodynamic quality of the solvent.

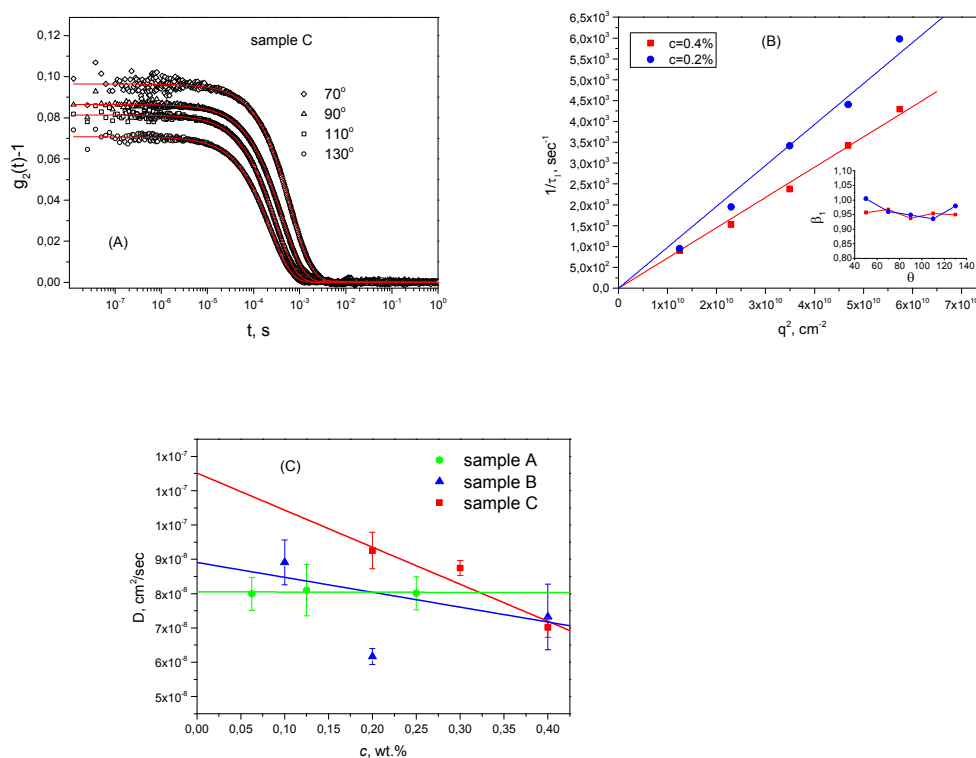


Figure 3. (A) Intensity autocorrelation functions for sample C at different angles measured by 3D-DLS method $T=40$ °C, $c=0.4$ wt.% (B) q^2 dependence of the inverse relaxation time of the fast mode (τ_1) for sample C. Inset: angle dependence of the stretching parameter β_1 (C) Concentration dependence of apparent diffusion coefficients from 3D-DLS experiments for the fast mode (τ_1).

3D-DLS experiments were conducted to obtain further information on size and dynamics of the nanoparticles and to investigate how apparent R_h is changing with increasing concentration at 40 °C. The intensity autocorrelation functions were fitted by double stretched exponential function ($A_1 \exp\left(-\left(\frac{t}{\tau_1}\right)^{\beta_1}\right) + A_2 \exp\left(-\left(\frac{t}{\tau_2}\right)^{\beta_2}\right) + B$) from where the values of relaxation times were extracted (Figure 3A). Stretching parameters β_1 and β_2 describe polydispersity for each mode. The possible range for the β value lasts from 0 (high polydispersity) to 1, for an ideal monodisperse case. Experiments were conducted in a broad range of scattering angles, corresponding to scattering wave vectors q^2 from $0.5 \cdot 10^{10}$ to $5.8 \cdot 10^{10} \text{ cm}^{-2}$. In vast majority cases, the obtained values for the amplitude for the second mode (A_2) were negligible (below 0.005). That finding together with chaotic changes of polydispersity parameter β_2 as a function of angle, sometimes even above 1, led us to conclusion to discard the second mode from consideration. For β_1 parameter, we have observed monotonous dependence in a range of 0.95-1.0 that indicates low polydispersity of nanoparticles (Figure 3B, Inset). The reverse relaxation times plotted for the fast mode (τ_1) as a function of q^2 indicate a diffusive nature of the relaxation process (Figure 3B) since $\frac{1}{\tau} = D_{app} q^2$, ref ²⁶. The values of apparent diffusion coefficients were calculated from the slope that were later depicted as a function of concentration (Figure 3C). From true values of diffusion coefficients calculated by extrapolation to infinite dilution, the true values of hydrodynamic radius were calculated for sample A, C, D. These values were different from the ones measured by conventional DLS method (Figure 2). The discrepancy could be attributed to the fact that conventional DLS data were measured at finite concentration. It is known³⁸ that in a dilute regime the concentration dependence of a translation diffusion coefficient can be written as $D_t(c) = D_0(1 + k_D c)$. Here k_D is a second hydrodynamic virial coefficient which is specific to a particular polymer-

solvent system and depends on a product of second virial coefficient and molecular weight $k_D = 2A_2M_w - k_f - \bar{v}$. Thus the higher the molecular weights, the higher the k_D . Static light scattering support the conclusion that molecular weight of nanoparticles formed at 40 °C is very high (Table 2, Supporting information).

Table2. Molecular weight, radius of gyration and second virial coefficient of nanoparticles at T=40 °C measured by SLS.

| | A | B | C | D |
|---|------|-----|------|-------|
| | SLS | SLS | SLS | SLS |
| $M_w, 10^6, \text{Da}$ | 8.6 | 5.8 | 28 | 42 |
| R_g, nm | 106 | 107 | 137 | 124 |
| $A_2, 10^{-9}$ $\text{mol}\cdot\text{dm}^3/\text{g}$ | -4.3 | 2.3 | 0.09 | -0.72 |

To get a deeper understanding of the internal structure of nanoparticles, NMR experiments were performed. The temperature dependence of a phase-separated fraction p , *i.e.* amount of polymer groups which take part in phase separation, was calculated for different groups (Figures 4, 5). The p value calculated for the CH_2 of PNIPAM backbone shows different behavior as a function of temperature for PNIPAM and PNIPAM-*b*-PEG-*b*-PNIPAM copolymers (Figure 4). Whereas for PNIPAM, p reaches its highest value in a very narrow temperature range, all copolymers have a much broader transition. Microphase separation for PNIPAM-*b*-PEG-*b*-PNIPAM copolymers is complex - a sharp increase is followed by gradual growth. For **C** (PNIPAM₅₄ - *b* - PEG₇₉ (D) - *b* - PNIPAM₅₄) and **D** (PNIPAM₅₁ - *b* - PEG₉₀ - *b* - PNIPAM₅₁), a first stage of transition takes place at 30 - 47 °C, with the second one at 47 - 60 °C (Figure 4A). For the backbone of block copolymers **A** (PNIPAM₃₀ - *b* - PEG₇₉ (D) - *b* - PNIPAM₃₀) and **B** (PNIPAM₃₈ - *b* - PEG₉₀ - *b* - PNIPAM₃₈), the first stage occurs at 30-57 °C, the second one at 57 - 60 °C.

A comparison of p values for the backbone and pendant groups shows that the main chain of all copolymers participates fully in phase separation, while the pendant groups of copolymers **A** and **B** collapse to the globule on 75% (Figure 4B). Nevertheless, for copolymers with longer PNIPAM chains- **C** and **D**- the p value at high temperatures shows complete phase separation for pendant groups.

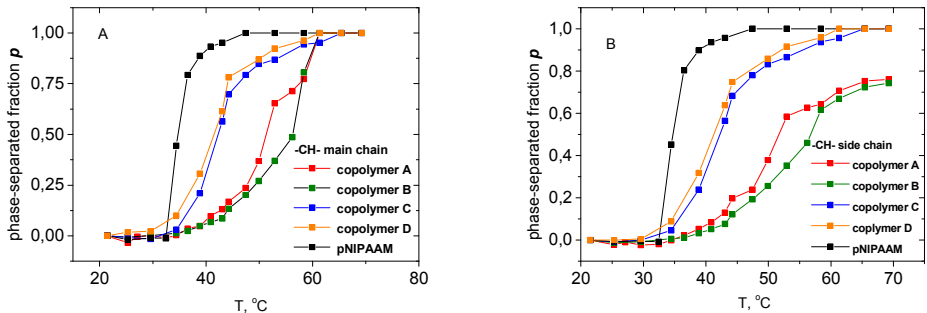


Figure 4. (A) Temperature dependence of the p -fraction as determined from integrated intensities of CH₂ band in ¹H NMR spectra of PNIPAM backbone. (B) Temperature dependence of the p -fraction as determined from integrated intensities of CH band in ¹H NMR spectra of PNIPAM pendant group.

Interestingly, PEG chains also participate in the phase-separation process (Figure 5). With increasing temperature, up to 30% of PEG groups was involved in phase separation. For the copolymers with longer PNIPAM block (**C** and **D**), the phase separation parameter for PEG groups is higher.

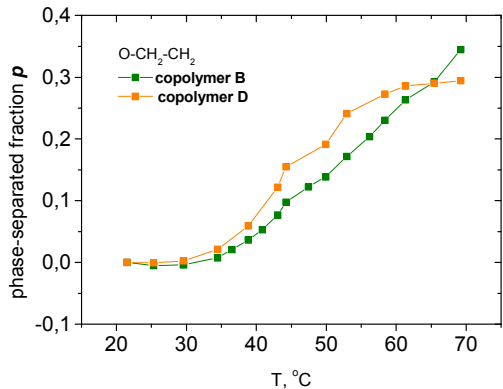


Figure 5. Temperature dependence of the *p*-fraction as determined from integrated intensities of PEG chains for block copolymer B and block copolymer D from ^1H NMR spectra.

Table 3. ^1H spin-spin relaxation times T_2 of CH_3 protons of a pendant group of PNIPAM, HDO molecules and CH_2 protons of PEG in D_2O solutions of PNIPAM-*b*-PEG-*b*-PNIPAM triblock copolymers.

| Temperature, $^{\circ}\text{C}$ | PNIPAM (s) | | | | HDO (s) | | | | PEG (s) | | | |
|------------------------------------|------------|-------|------|------|---------|------|------|------|---------|------|------|------|
| | A | B | C | D | A | B | C | D | A | B | C | D |
| 22 | 0.16 | 0.166 | 0.14 | 0.13 | 7.56 | 2.26 | 3.04 | 3.13 | 0.55 | 0.51 | 0.56 | 0.51 |
| 67 | 0.25 | 0.329 | 0.71 | 0.24 | 4.72 | 4.28 | 2.90 | 3.00 | 1.17 | 0.91 | 1.05 | 0.76 |

The local mobility data obtained from NMR experiments are in agreement with conclusions based on *p* value. Below the CPT, PEG chains are very mobile and T_2 relaxation time is not influenced by the presence of the different terminal PNIPAM blocks (Table 3). It is known that, ^1H spin-spin relaxation time T_2 of a specific group is proportional to its mobility, therefore PNIPAM chains are obviously much slower than PEG below CPT. The same conclusion is valid for the case above the CPT, where the similar difference between the relaxation times of PEG and PNIPAM was observed. Here it should be noted that T_2 values reported in Table 3 for PNIPAM at 67°C correspond only to a small fraction of groups that are still mobile and not involved in phase separation.

SANS

SANS experiments were conducted at 25°C (below CPT) and 40°C (above CPT). The experimental curves for all four samples are presented in Figure 6. The behavior of scattering curves at 25°C was examined first and were showing two features: a significant upturn at low $q < 0.2 \text{ nm}^{-1}$ and smooth decrease at $0.2 < q < 0.8 \text{ nm}^{-1}$. The scattered intensity for the first region for samples A and B at $q < 0.2 \text{ nm}^{-1}$ obeys a power law with $I \sim q^{-3.3}$ that corresponds

to structures with a loose surface (Figure 6A). Scatterers in samples C and D have sharp interface since they manifest classical Porod behavior $I \sim q^{-4.0}$ (Figure 6B). The same approach in a q range $q > 0.2 \text{ nm}^{-1}$ reveals power law of $I \sim q^{-1.7}$. This dependency is typical for Gaussian chains with excluded volume effects. Thus, it is possible to assume that the SANS curves below CPT contain the scattering from two different structures that could be fitted by a combination of two contributions - generalized Gaussian chain form factor and mass fractal form factor: $I(q) = P_{\text{GGC}}(q) + P_{\text{MF}}(q)$. The scattering function for the generalized Gaussian coil could be written as:

$$P_{\text{GGC}}(q) = I_0^c \frac{U^{\frac{1}{2\nu}} \Gamma\left(\frac{1}{2\nu}\right) - \Gamma\left(\frac{1}{\nu}\right) - U^{\frac{1}{2\nu}} \Gamma\left(\frac{1}{2\nu}, U\right) + \Gamma\left(\frac{1}{\nu}, U\right)}{\nu U^{1/\nu}}$$

here, $U = (2\nu + 1)(2\nu + 2) \frac{q^2 R_g^2}{6}$, and $\Gamma\left(\frac{1}{2\nu}\right)$ – Gamma function.

The mass fractal form factor can be described as:

$$P_{\text{MF}}(q) = 4\pi I_0^a \int_0^\infty r^{D-3} h(r, R) \frac{\sin(qr)}{qr} r^2 dr$$

$h(r, R) = \exp\left[-\frac{Dr^2}{R_g^2}\right]$ is a cut-off function.

The choice of Gaussian chain form factor is obvious since we can expect such behavior for a single polymer chain below CPT. Concerning mass fractal contribution, there were several models which plausibly describe scattering curves at $q < 0.2 \text{ nm}^{-1}$, such as polydisperse hard spheres, fractal aggregates, *etc.*, however, mass fractal contribution gave the best fitting results. The mass fractal contribution is attributed to a small fraction of aggregates observed by DLS. Six general parameters were used in the fitting procedure; form factor: R_g^c – radius of gyration of chain, ν – excluded volume parameter or Flory exponent and I_0^c – forward scattering of chain, and mass fractal form factor with parameters: I_0^a – forward scattering of fractal aggregates, R_g^a – radius of gyration of fractal aggregates, D – fractal dimension. Results from the fit of experimental curves are shown in Table 4 and Figure 7.

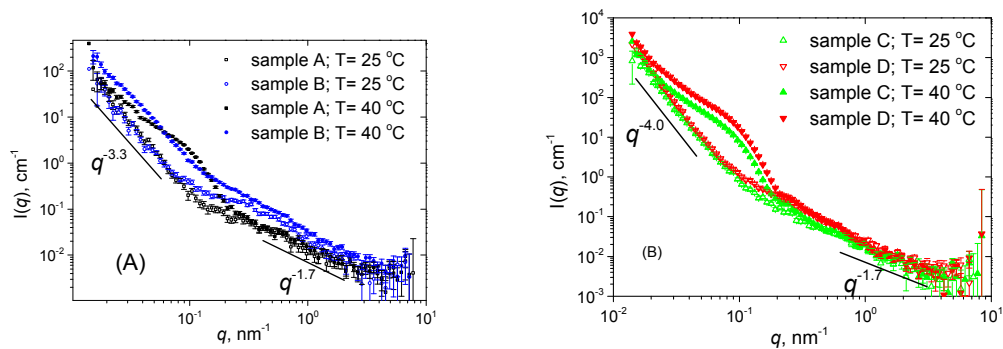


Figure 6. SANS data for PNIPAM-*b*-PEG-*b*-PNIPAM copolymers at 25 °C and 40 °C. (A) block copolymers A and B (B) block copolymers C and D.

Table 4. Fitting parameters for copolymers at 25 °C.

| | A | B | C | D |
|--|-----------|-----------|-----------|-----------|
| Form Factor: Generalized Gaussian Coil | | | | |
| R_g^c , nm | 3.5±0.1 | 4.3±0.3 | 2.1±0.1 | 4.8±0.1 |
| ν | 0.8±0.2 | 0.58±0.07 | 0.6±0.2 | 0.62±0.08 |
| I_0^s , cm ⁻¹ | 0.06±0.01 | 0.17±0.01 | 0.04±0.01 | 0.19±0.02 |
| Structure Factor: Mass Fractal | | | | |
| R_g^a , nm | 66.7±0.1 | 97.5±0.1 | 105.0±0.1 | 105.8±0.1 |
| D | 2.58±0.02 | 2.51±0.02 | 2.75±0.01 | 2.78±0.01 |
| I_0^a , cm ⁻¹ | 34.4±0.1 | 82.9±0.1 | 1170±1 | 1832±1 |

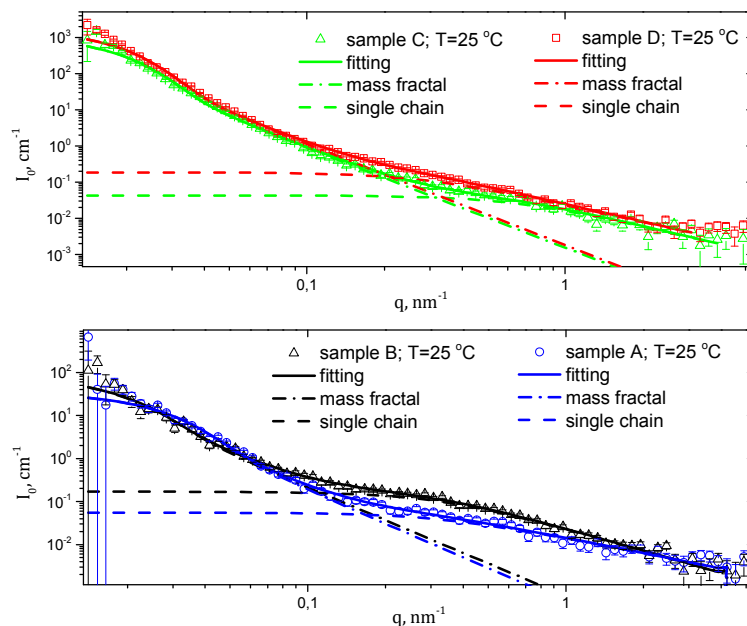


Figure 7. SANS data for polymers at 25 °C with results from the fitting procedure. Solid lines are fits.

The data obtained from the fitting procedure with those that coming from the description of chemical structure can now be compared. Several dependences could be pointed out. These features could be analyzed on different levels: on the level of single polymer chain, individual scatterers or entire particles. We shall begin our consideration with the level of polymer chain. While for the low molecular weight polymers (**A** and **B**, roughly 10-12 kDa), the variation in the length of thermoresponsive and hydrophilic block does not have significant effect on the gyration radius of single polymer chain, and the opposite was observed when molecular weight of polymer exceed 15 kDa (**C** and **D**). Thus, if we take the dimension of low molecular weight polymers as a reference, it becomes clear that the increase in the length of thermoresponsive block results in the formation of a more compact structure, even at temperature below the transition point. On the contrary, the increase in the length of

hydrophilic block leads to a growth in the dimensions of polymer chain. The Flory exponent value of around 0.6 obtained from Generalized Gaussian Coil model for all polymers can be attributed to a swollen conformation of the polymer chain; water is a thermodynamically good solvent for our solutions at that particular temperature. Another feature appears when we compare the radius of individual scatterers from the structure factor with the corresponding radius of gyration of polymer chain from the form factor (Table 4). While these values are close to each other for polymers **C** and **D**, the values from structure factor for polymers **A** and **B** exceed the values from form factor at least in two times. One can assume, the excluded volume has to be taken into account when the polymers **A** and **B** are analyzed. Interestingly, the inverse correlation occurred, if we compare the content of PNIPAM groups in polymer with dimension of individual scatters taken from the fitting results. The longer the PNIPAM block is, the smaller size of single scatter was determined. At the same time, on the level of whole particle, there is a well-defined relation between number of PEG units and dimension of whole aggregate. The increase in the length of PEG block results in increase in the size of entire aggregates. These aggregates are characterized by 2.5-2.7 fractal dimension that corresponds to the loose cluster objects.

If we apply the same strategy to the analysis of scattering curves recorded at 40 °C, one more feature should be considered in the interpretation of the experimental data; the shoulder appears at $0.03 < q < 0.2 \text{ nm}^{-1}$. This shoulder is visible for every polymer and can be analyzed as a result of the transition process from a molecular state of polymer at 25 °C to an aggregate state at 40 °C. It has to be mentioned, the appearance of this shoulder in the scattering curve diminishes partly the first region, where the significant decrease in intensity was observed recently for curves at 25 °C, but it is still detectable at $q < 0.03 \text{ nm}^{-1}$. Thus, there are three distinct regions here: $q < 0.03 \text{ nm}^{-1}$, $0.03 < q < 0.2 \text{ nm}^{-1}$ and $q > 0.2 \text{ nm}^{-1}$. Application of the power law in this case gives the following results: $I_0 \sim q^{-1.4}$ for $q > 0.2 \text{ nm}^{-1}$. Definition of the

power law at values of q less than 0.03 nm^{-1} is complicated by the presence of only a few points in the region. Therefore, one can conclude that we are dealing with a very similar system. The only differences are a more compact sphere and stretched polymer chains in this particular case. For the purpose of quantitative analysis several different models have been tried for fitting. All of these models were a combination of certain form factor with MassFractal structure factor. Among form factors which were applied, i.e.: hard sphere, generalized Gaussian coil, sphere with exponential shell, sphere with attached Gaussian chains, Dozier model, the Beucage model, the only model was successful in describing the behavior of scattering curves was the Beucage mode³⁹ (Figure 8, Table 5).

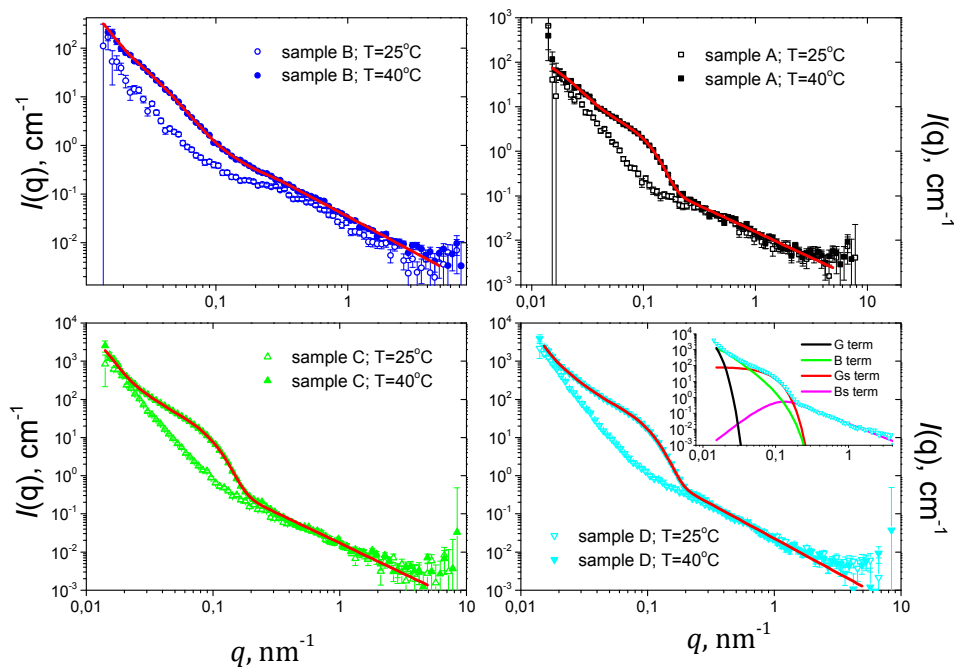


Figure 8. SANS data for every single polymer at 25 and 40 °C. Solid red lines are fits by the Beucage model. Inset for sample D: separated contributions according to the Beucage model.

Table 5. Fitting parameters for copolymers at 40 °C.

| Fitting parameter of Beucage model | A d-PEG | B h-PEG | C d-PEG | D h-PEG |
|--|-------------------------------|---------------------------------|-------------------------------|-------------------------------|
| G | 278 | 2061 | 15057 | 58845 |
| B | $(1.2 \pm 1.0) \cdot 10^{-4}$ | $(1.30 \pm 0.05) \cdot 10^{-2}$ | $(4 \pm 1) \cdot 10^{-3}$ | $(3.5 \pm 0.1) \cdot 10^{-3}$ |
| G_s | 6.2 ± 0.2 | 1.60 ± 0.03 | 40.2 ± 0.2 | 80.18 ± 0.01 |
| B_s | $(1.6 \pm 0.1) \cdot 10^{-2}$ | $(3.5 \pm 0.1) \cdot 10^{-2}$ | $(1.7 \pm 0.1) \cdot 10^{-2}$ | $(2.3 \pm 0.1) \cdot 10^{-2}$ |
| R_{LS} , nm | 156.5 ± 0.2 | 203.9 ± 0.1 | 184.6 ± 0.1 | 221.5 ± 0.1 |
| R_{sub} , nm | 20 ± 1 | 25.17 ± 0.01 | 14.54 ± 0.04 | 16.9 ± 0.1 |
| R_s , nm | 19.5 | 15.88 ± 0.02 | 24.27 ± 0.02 | 22.8 ± 0.1 |
| D | 3.4 ± 0.1 | 2.3 ± 0.1 | 2.9 ± 0.1 | 3.15 ± 0.02 |
| D_s | 1.17 ± 0.03 | 1.46 ± 0.01 | 1.58 ± 0.04 | 1.80 ± 0.03 |
| χ^2 | 67.9 | 69.4 | 98.6 | 106.7 |

The Beucage model describes fractal aggregates consisting of smaller particles:

$$I_{BC}(q) = G \exp\left(-\frac{q^2 R_{LS}^2}{3}\right) + B \exp\left(-\frac{q^2 R_{sub}^2}{3}\right) \left(\frac{[\text{erf}(q R_s / \sqrt{6})]^3}{q}\right)^D + G_s \exp\left(-\frac{q^2 R_s^2}{3}\right) + B_s \left(\frac{[\text{erf}(q R_s / \sqrt{6})]^3}{q}\right)^{D_s}$$

The fitting parameters for the model are G - the Guinier pre-factor of the larger structure, B - a pre-factor specific to the type of power-law scattering, G_s - the Guinier pre-factor of the smaller structure, B_s - a pre-factor specific to the type of power-law scattering, R_{LS} - large-scale structure, R_{sub} - surface-fractal cut-off radius of gyration, R_s - size of small subunits, D - scaling exponent of the power law assigned to the larger structure R_g , D_s - scaling exponent of the power law assigned to the smaller structure R_s .

There are nine fitting parameters in the Beucage model described above, and whilst all values obtained from the fitting procedure are rationalisable, we cannot completely exclude the possibility that another model could also describe the SANS data. This hypothetical model should have a similar hierarchical structure, in order to describe such a complex system.

At 40 °C, nanoparticles made of copolymer A and C have overall radius of 156 and 185 nm, respectively, consisted of small 20.3 and 14.5 nm particles, that are arranged inside of a fractal with scaling power law 3.36 and 2.89 (surface fractal). Inside of small particles, they behave as polymers with some excluded volumes effect (scaling power laws are 1.17 and 1.58) (Figure 9). Nanoparticles made of copolymers B and D are somewhat bigger than the ones composed of A and C due to protonated PEG.

NMR, DLS, and SANS data together provide an opportunity to describe nanoparticles formation in details. Below CPT, triblock copolymers exist in solution as single molecules

together with a small fraction of large aggregates as it nicely seen by DLS and SANS. Analysis of T_2 data from NMR shows that PNIPAM blocks are less mobile in comparison with a middle PEG block. Formation of nanoparticles starts from occurrence of small domains formed by PNIPAM blocks since they disappear from NMR spectrum. In contrast with pure PNIPAM, nanoparticles formation for PNIPAM-*b*-PEG-*b*-PNIPAM expands over broader temperature range and such broadening depends on the length of PEG chain. p -fraction value extracted from NMR data proves that mobile PEG chains significantly retard fast phase separation process. Nevertheless, at temperature much higher than CPT up to 100% of all PNIPAM monomers could be inside of domains. The overall structure of nanoparticles formed above CPT could be described on a large scale a surface fractal structure. PNIPAM domains were visualized by SANS contrast variation study by using deuterated PEG block.

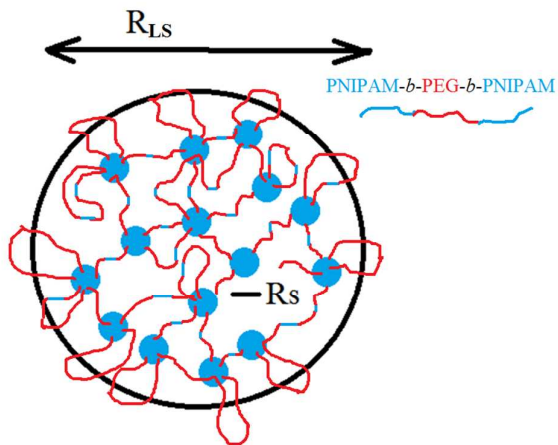


Figure 9. Hypothetical structure of nanoparticles above CPT.

CONCLUSIONS

For the first time, the onset of nanoparticles formation above CPT of PNIPAM-*b*-PEG-*b*-PNIPAM block copolymers have been analyzed in aqueous solutions in depth. The findings can be summarized as follows: below CPT, triblock copolymers exist in solution as single molecules together with a small fraction of large aggregates. PNIPAM blocks are less mobile in comparison with a middle PEG block. Formation of nanoparticles with hierarchical structure was observed above CPT. The nanoparticles could be described on a large scale a

1
2
3 surface fractal structure. On a short scale nanoparticles consist of small domains of partially
4
5 phase-separated PNIPAM blocks interconnected by mobile PEG chains. Such domains were
6
7 visualized by SANS contrast variation study by using deuterated PEG block. Further increase
8
9 in temperature above CPT leads to higher immobilization of PNIPAM blocks inside of
10
11 domains up to 100% of all monomer units.
12
13
14
15
16
17
18

19 ASSOCIATED CONTENT

20 21 **Supporting Information**

22
23
24
25
26 Synthesis of PEG macroinitiator. Synthesis of ME₆TREN. Guinier plot for the sample C. A
27
28 Guinier plot for the sample B; Temperature 40°C. Guinier plot for the sample D; Temperature
29
30 40°C
31

32 This material is available free of charge via the Internet at <http://pubs.acs.org>.”
33
34

35 AUTHOR INFORMATION

36
37
38 Corresponding Author (**Sergey Filippov**)
39

40
41 *Tel: +420-608720561; Fax: +420-296809410
42

43
44 E-mail: sfill225@gmail.com
45

46
47 Corresponding Author (**Michael T. Cook**)
48

49 *Tel: +44 (0)170 728 3439
50

51
52 E-mail: m.cook5@herts.ac.uk
53
54
55

56
57 Author Contributions
58
59
60

1
2
3
4
5
6
7
8
9
10
11
12
13
14
15
16
17
18
19
20
21
22
23
24
25
26
27
28
29
30
31
32
33
34
35
36
37
38
39
40
41
42
43
44
45
46
47
48
49
50
51
52
53
54
55
56
57
58
59
60

The manuscript was written through contributions of all authors. All authors have given approval to the final version of the manuscript.

Notes

The authors declare no competing financial interest.

ACKNOWLEDGMENTS

The ISIS (Didcot, UK) is thanked for granting SANS beam time (experiment number 1410107). S.F. acknowledges the Czech Science Foundation Grant No. 15-10527J. The authors acknowledge support from the European Union under the Framework 7 program under a contract from an Integrated Infrastructure Initiative (Reference 262348, ESMI). S.F. thanks Ms. Panagiota Bogri and Dr. George Petekidis for their help with 3D-DLS experiments. The authors acknowledge Chemical Analysis Facility (University of Reading) for providing access to NMR spectroscopy used in the analysis of chemical structure of triblock copolymers.

REFERENCES

(1) Aseyev, V.; Tenhu, H.; Winnik, F. M. Non-ionic Thermoresponsive Polymers in Water. *Adv. Polym. Science* **2011**, 242, 29-89.

(2) Wang, X.; Wu, C. Light-Scattering Study of Coil-to-Globule Transition of a Poly(N-isopropylacrylamide) Chain in Deuterated Water. *Macromolecules* **1999**, 32, 4299-4301.

(3) Prabakaran, M.; Grailer, J. J.; Steeber, D. A.; Gong, S. Q. Thermosensitive micelles based on folate-conjugated poly(N-vinylcaprolactam)-block-poly(ethylene glycol) for tumor-targeted drug delivery. *Macromol. Biosci.* **2009**, *9*, 744–753.

(4) Hruby, M.; Konak, C.; Kucka, J.; Vetrik, M.; Filippov, S.K.; Vetvicka, D.; Mackova, H.; Karlsson, G.; Edwards, K.; Rihova, B.; Ulbrich, K. Thermoresponsive, Hydrolytically Degradable Polymer Micelles Intended for Radionuclide Delivery. *Macromol. Biosci.* **2009**, *9*, 1016-1027.

(5) Hruby, M.; Filippov, S.K.; Panek, J.; Novakova, M.; Mackova, H.; Kucka, J.; Ulbrich, K. Thermoresponsive micelles for radionuclide delivery. *J Control. Release.* **2010**, *148*, E60-E62.

(6) Hruby, M.; Filippov, S.K.; Panek, J.; Novakova, M.; Mackova, H.; Kucka, J.; Vetvicka, D.; Ulbrich, K. Polyoxazoline Thermoresponsive Micelles as Radionuclide Delivery Systems. *Macromol. Biosci.* **2010**, *10*, 916-924.

(7) Panek, J.; Filippov, S.K.; Hruby, M.; Rabyk, M.; Bogomolova, A.; Kucka, J.; Stepanek, P. Thermoresponsive Nanoparticles Based on Poly(2-alkyl-2-Oxazolines) and Pluronic F127. *Macromol. Rap. Com.* **2012**, *33*, 1683-1689.

(8) Bogomolova, A.; Hruby, M.; Panek, J.; Rabyk, M.; Turner, S.; Bals, S.; Steinhart, M.; Zhigunov, A.; Sedlacek, O.; Stepanek, P.; Filippov, S.K. Small-angle X-ray scattering and light scattering study of hybrid nanoparticles composed of thermoresponsive triblock copolymer F127 and thermoresponsive statistical polyoxazolines with hydrophobic moieties. *J. Appl. Crystal.* **2013**, *46*, 1690-1698.

- (9) Laga, R.; Janouškova, O.; Ulbrich, K.; Pola, R.; Blazkova, J.; Filippov, S.K.; Etrych T.; Pechar, M. Thermo-responsive polymer micelles as nano-sized pharmaceuticals for cancer therapy, *Biomacromolecules* **2015**, *16*, 2493–2505.
- (10) Bogomolova, A.; Filippov, S.K.; Starovoytova, L.; Angelov, B.; Konarev, P.; Svergun, D. I.; Sedlacek, O.; Hruby, M.; Stepanek, P. Study of Study of Thermosensitive Amphiphilic Poly-Oxazolines of Complex Nature and Their Interaction with Ionic Surfactants. Hydrophobic, Thermosensitive and Hydrophilic Moieties: Are They Equally Important? *J Phys. Chem. B* **2014**, *118*, 4940-4950.
- (11) Duval, M.; Waton, G.; Schosseler, F. Temperature-induced growth of wormlike copolymer micelles. *Langmuir* **2005**, *21*, 4904–4911.
- (12) Escobar-Chávez, J. J.; López-Cervantes, M.; Naik, A.; Kalia, Y.N.; Quintanar-Guerrero, D.; Ganem-Quintanar, A. Applications of thermo-reversible pluronic F-127 gels in pharmaceutical formulations. *J. Pharm. Pharm. Sci.* **2006**, *9*, 339–358.
- (13) He, C.; Kim, S. W.; Lee, D. S. In situ gelling stimuli-sensitive block copolymer hydrogels for drug delivery. *J. Control. Release.* **2008**, *127*, 189–207.
- (14) Hoogenboom, R.; Thijs, H.M.L.; Jochems, M.J.H.C.; van Lankvelt, B.M.; Fijten, M.W.M.; Schubert, U.S. Tuning the LCST of poly(2-oxazoline)s by varying composition and molecular weight: alternatives to poly(N-isopropylacrylamide)? *Chem. Commun. (Camb).* **2008**, 5758–5760.
- (15) Topp, M. D. C.; Dijkstra, P. J.; Talsma, H.; Feijen, J. Thermosensitive Micelle-Forming Block Copolymers of Poly(ethylene glycol) and Poly(N-isopropylacrylamide). *Macromolecules* **1997**, *30*, 8518–8520.

- (16) Virtanen, J.; Holappa, S.; Lemmetyinen, H.; Tenhu, H. Aggregation in Aqueous Poly(N-isopropylacrylamide)-block-poly(ethylene oxide) Solutions Studied by Fluorescence Spectroscopy and Light Scattering. *Macromolecules* **2002**, *35*, 4763–4769.
- (17) Zhu, P. Particle formation and aggregation - collapse behavior of poly (N - isopropylacrylamide) and poly (ethylene glycol) block copolymers in the presence of cross-linking agent. *J Mater Sci Mater Med.* **2004**, *5*, 567–573.
- (18) Zhang, W.; Shi, L.; Wu, K.; An, Y. Thermoresponsive Micellization of Poly (ethylene glycol)-b -poly (N-isopropylacrylamide) in Water. *Macromolecules* **2005**, 5743–5747.
- (19) Zhao, J.; Zhang, G.; Pispas S. Morphological transitions in aggregates of thermosensitive poly(ethylene oxide)-b-poly(N-isopropylacrylamide) block copolymers prepared via RAFT polymerization. *J. Polym. Sci. Part A: Polym. Chem.* **2009**, *47*, 4099e110.
- (20) Papagiannopoulos, A.; Zhao, J.; Zhang, G.; Pispas, S.; Radulescu, A. Thermoresponsive transition of a PEO-b-PNIPAM copolymer: From hierarchical aggregates to well defined ellipsoidal vesicles. *Polymer*, **2013**, *54*, 6373-6380.
- (21) Lin, H. H.; Cheng, Y. L. In-situ thermoreversible gelation of block and star copolymers of poly(ethylene glycol) and poly(n-isopropylacrylamide) of varying architectures. *Macromolecules* **2001**, *34*, 3710–3715.
- (22) Teodorescu, M.; Negru, I.; Stanescu, P.O.; Drghici, C., Lungu, A., Sarbu, A.c Thermogelation properties of poly(N-isopropylacrylamide) – block – poly(ethylene glycol) – block – poly(N-isopropylacrylamide) triblock copolymer aqueous solutions. *React. Funct. Polym.* **2010**, *70*, 790–797.
- (23) De Graaf, A.J.; Boere, K.W.; Kemmink, J.; Fokkink, R.G.; van Nostrum, C.F.; Rijkers, D.T.; van der Gucht, J.; Wienk, H.; Baldus, M.; Mastrobattista, E.; Vermonden, T.; Hennink,

W.E. Looped structure of flowerlike micelles revealed by ^1H NMR relaxometry and light scattering. *Langmuir* **2011**, 27, 9843-9848.

(24) Radecki, M.; Spěvák, J.; Zhigunov, A.; Sedláková, Z.; Hanyková, L. Temperature-induced phase transition in hydrogels of interpenetrating networks of poly(N-isopropylacrylamide) and polyacrylamide. *Eur. Polym. J.* **2015**, 68, 68-79.

(25) Uřilová, H.; Čtástná, J.; Nyková, L.; Dláková, Z.; Spěvák, J. ^1H NMR study of temperature-induced phase separation in solutions of poly(N-isopropylmethacrylamide-co-acrylamide) copolymers. *Eur. Polym. J.* **2010**, 46, 1299-1306.

(26) Spěvák, J. NMR investigations of phase transition in aqueous polymer solutions and gels. *Cur. Opin. Colloid. Interf. Sci.* **2009**, 14, 184-191.

(27) http://www.mantidproject.org/Main_Page

(28) Wignall, G. D.; Bates, F. S. Absolute calibration of small-angle neutron scattering data. *J. Appl. Crystallogr.* **1987**, 20, 28-40.

(29) Pecora, R. Dynamic Light Scattering: Applications of Photon Correlation Spectroscopy, Plenum Press, **1985**.

(30) B. Chu, Laser Light Scattering: Basic Principles and Practice, Academic Press, Inc. New York, **1991**.

(31) Urban, C.; Schurtenberger, P. Characterization of turbid colloidal suspensions using light scattering techniques combined with cross-correlation methods, *J. Colloid Interf. Sci.* **1998**, 207, 150-158.

(32) Scheffold, F.; Schurtenberger, P. Light scattering probes of viscoelastic fluids and solids, *Soft Mater.* **2003**, 1, 139-165.

- (33) Pusey, P.N., Suppression of multiple scattering by photon cross-correlation techniques, *Cur. Opin. Colloid Interf. Sci.* **1999**, *4*, 177-185.
- (34) Ye, J.; Narain, R. Water-assisted atom transfer radical polymerization of N-isopropylacrylamide: nature of solvent and temperature. *J. Phys. Chem. B.* **2009**, *113*, 676–681.
- (35) Pospisilova, A.; Filippov, S. F.; Bogomolova, A.; Turner, S.; Sedlacek, O.; Matushkin, N.; Cernochova, Z.; Stepanek P.; Hruby, M. Glycogen-graft-poly(2-alkyl-2-oxazolines) – the new versatile biopolymer-based thermoresponsive macromolecular toolbox. *RSC Adv.* **2014**, *4*, 61580-61588.
- (36) Virtanen, J.; Baron, C.; Tenhu, H. Grafting of poly(N-isopropylacrylamide) with poly(ethylene oxide) under various reaction conditions. *Macromolecules* **2000**, *33*, 336-341.
- (37) Aseyev, V.; Hietala, S.; Laukkanen, A.; Nuopponen, M.; Confortini, O.; Du Prez, F.E.; Tenhu, H. Mesoglobules of thermoresponsive polymers in dilute aqueous solutions above the LCST. *Polymer* **2005**, *46*, 7118-7131.
- (38) Yamakawa, H. Modern Theory of Polymer Solutions (Harper and Row, New York, **1971**).
- (39) Beaucage, G. Approximations leading to a unified exponential/power-law approach to small-angle scattering. *J. Appl. Cryst.* **1995**, *28*, 717-728.

For Table of Contents Use Only

Title: Internal nanoparticle structure of temperature responsive self-assembled PNIPAM-*b*-PEG-*b*-PNIPAM triblock copolymers in aqueous solutions: NMR, SANS and Light Scattering studies

Authors: Sergey K. Filippov, Anna Bogomolova, Leonid Kabarov, Nadiia Velychkivska, Larisa Starovoytova, Zulfiya Cernochova, Sarah E. Rogers, Wing Man Lau, Vitaliy V. Khutoryanskiy, Michael T. Cook

